Journal of Power Sources 261 (2014) 356–362

Contents lists available at ScienceDirect

Journal of Power Sources

journal homepage: www.elsevier.com/locate/jpowsour

Optimization of primary printed batteries based on Zn/MnO_2

E. Madej [a,b], M. Espig [c], R.R. Baumann [c], W. Schuhmann [a,*], F. La Mantia [b,*]

[a] Analytische Chemie – Elektroanalytik & Sensorik, D-44780 Bochum, Germany
[b] CES – Zentrum für Elektrochemie, Ruhr-Universität Bochum, D-44780 Bochum, Germany
[c] Institut für Print- und Mediatechnik, Technische Universität Chemnitz, D-09126 Chemnitz, Germany

HIGHLIGHTS

- The distribution of overvoltage in a thin-film printed battery is different than in a typical battery.
- Electrochemical impedance spectroscopy can be used to identify the distribution of overvoltage.
- Thin-film batteries printed on paper have as main limitation the conductivity of the current collector.
- By increasing the thickness of the carbon current collector, the power density of the battery was increased by 4 times.

ARTICLE INFO

Article history:
Received 11 June 2013
Received in revised form
13 December 2013
Accepted 22 March 2014
Available online 30 March 2014

Keywords:
Printed batteries
Manganese dioxide/zinc batteries
Electrochemical impedance spectroscopy
Current collector

ABSTRACT

Thin-film batteries based on zinc/manganese dioxide chemistry with gel $ZnCl_2$ electrolyte were manufactured as single (1.5 V) and double (3.0 V) cells from electrodes printed on paper substrates covered with different polymeric insulating coatings. Their properties were evaluated by means of electrochemical impedance spectroscopy and chronopotentiometry. Best performing cells achieved capacities in the range of 3 mAh cm^{-2} during discharge with 100 μA current, corresponding approximately to C/100 discharge rate. The influence of the cell elements on the overvoltage was examined and suggestions for the optimization of their performance were postulated. In particular, it was observed that limitations in the delivered power were governed by the poor conductivity of the carbon current collector. An optimized cell was built and showed a 4-fold improvement in the power delivered at 1 mA.

1. Introduction

The concept of printed energy-storage devices has proven to work [1–5] and such systems are used nowadays in low power applications like smart sensors, greeting cards, medical strips and interactive packaging, while for future and target applications powering of flexible displays, RFID chips and even electric vehicles (EV) are envisaged. Main advantages of printed, so called thin-film batteries are their low weight (~1 g) and thickness in the range of 1 mm thanks to the application of the printing technology. Printed thin-film batteries were reported based on zinc/manganese dioxide [5,6], zinc/air [7], zinc/silver [8], nickel/hydrogen [9], nickel/metal hydride [5], lithium ion [2,10], and recently, organic radical [11] chemistries. Different flexible current collectors have been investigated including textiles [12–14], e.g. cotton fabric [15] or polyester fiber [16], plastics [3,13] and paper [2,10] used as a substrate covered with either different metal films (copper, aluminum and silver nanowires) or carbon nanotubes (CNTs) [2,3,10,13]. The latter appeared to be especially attractive due to their inherent high conductivity at concomitantly light weight. Low cost is reached due to both cheap components and the used inexpensive printing technology. Yet, the performances of printed batteries are far below the performances of corresponding classic batteries, due to changes in the distribution of the overvoltage inside the device. Further work is needed to optimize different elements of printed batteries in order to maximize the utilization of their theoretical capacity and improve the maximum deliverable power.

Electrochemical impedance spectroscopy (EIS) is a technique widely used in battery industry and research allowing for the evaluation of the performance and rate capability of batteries and their lifetime predictions [15–20]. Aging processes and decrease in performance have been linked to the rise in the internal resistance of battery components. EIS can also distinguish between ionic and electronic sources of the internal resistance of the battery, thus

* Corresponding authors.
E-mail addresses: wolfgang.schuhmann@rub.de (W. Schuhmann), fabio.lamantia@rub.de (F. La Mantia).

http://dx.doi.org/10.1016/j.jpowsour.2014.03.103
0378-7753/

allowing for optimization of the device during the manufacturing process.

The fabrication of printed batteries is accomplished by using screen-printing with a semi-automatic sheet-to-sheet unit. This technology enables the imprint of larger thicknesses and almost every material by using special inks [21]. Since the goal in battery production is to achieve rough electrode layers with the highest amount of active material, screen-printing appears to be a very attractive technique for the use of highly viscous inks [22]. The printing image is generated by a mask and an adequate mesh which are strung over an aluminum rack. The final printable areas are the open regions that had been washed out after photochemical development of the mask layer within the mesh [23]. A so-called stencil can be generated either inside the mesh opening or additionally as a cover layer to the mesh [24]. The properties of the used fibers determine the morphology of the prints. Monofilament polyester fibers are commonly used to build up regular screens because of their ductility and chemical resistivity towards a variety of ink formulations [25]. The number of filaments and the thread diameter define the mesh thickness, its opening degree and therefore also the ink volume that is transferred during printing.

In this work, we investigated printed batteries based on traditional zinc/manganese dioxide chemistry, all containing the same amount of active material and the same volume of printed electrolyte. The influence of the polymer coating of the paper substrate on the electrochemical performance of the devices was investigated by means of galvanostatic discharge (GD) and electrochemical impedance spectroscopy (EIS). Electrochemical tests were complemented by post-mortem analysis of the batteries including electric resistance measurements. The purpose of this work was to identify the factors limiting the power delivered by the printed battery. Based on the obtained results, an optimization of the printing process could be proposed aiming on an increase of the maximum power.

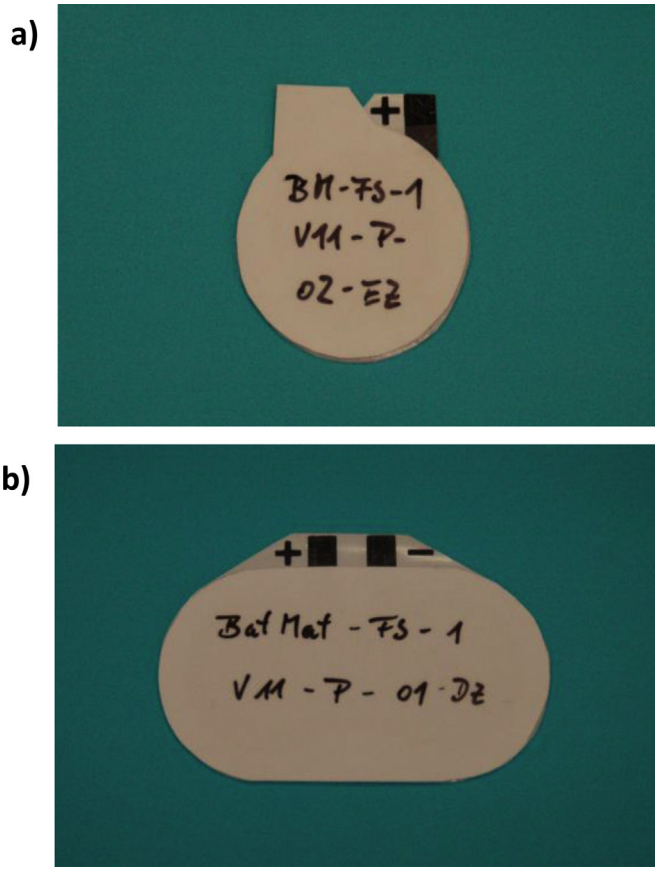

Fig. 1. Printed batteries in (a) single cell (1.5 V) and (b) double cell (series configuration; 3.0 V).

2. Experimental

Printed batteries based on the traditional zinc/manganese dioxide chemistry using $ZnCl_2$ as gel electrolyte [26] were manufactured at Technical University of Chemnitz in the form of single cells (1.5 V) and double cells in series configuration (3.0 V) as shown in Fig. 1. All cells contained the same amount of active materials and the same volume of electrolyte for comparison. Printing was done on a variety of paper substrates differing in the external polymer coating. The paper substrates were obtained from Schoeller Technocell GmbH & Co. KG and were named FS-1, FS-2, and FS-3, respectively. FS-1 was a raw paper extrusion coated with a polyethylene layer on both sides [27]. The printing surface was coated additionally with a hydrophilic polymer as primer on top and the total base weight of this paper is 200 g m^{-2}. FS-2 was a thinner paper extrusion coated with polypropylene on both sides, bearing no additional primer layer with a total base weight of 108 g m^{-2}. FS-3 again was extrusion coated with polyethylene on both sides without primer with a base weight of 120 g m^{-2}. The separator was obtained by perforation of a thin polymeric film with a laser.

The different components of the paper battery were applied separately layer by layer. In the first step current collectors made out of commercial carbon ink (Electrodag PF407C from Henkel) were printed on FS-substrates utilizing a table top screen printer Ekra E1-XL. The carbon ink formulation has not been changed before printing and a layer thickness of 4 μm was achieved in the FS-1 to FS-3 batteries, while a thickness of 30 μm was achieved in the case of the optimized battery. Regarding the plastic batteries, a carbon layer thickness of 25 μm was achieved. The ink consists of 36 w% of solid content and has an average density of 1.12 kg l^{-1}. Its viscosity is around 45 Pa s, sheer thinning during printing. After drying of the first coating with a continuous-flow dryer (3DMM microDRY), positive and negative electrode materials were printed. Inks based on zinc (as the active anode material) and manganese dioxide (as the active cathode material) were formulated to contain high amount of solid particles. The anode ink was composed of Typ-1 zinc, provided by Grillo Werke, showing a spattered morphology with spherical and elongate particles with a size distribution of d50 = 39 μm, mixed with carbon ink (as above) and 4-hydroxy-4-methyl-2-pentanone. The cathode ink was made up of Manganese(IV) oxide provided by Merck, showing a sliver morphology with smaller and bigger splints ranging from 5 to 30 μm mixed with distilled water, carbon ink (as above) and 4-hydroxy-4-methyl-2-pentanone. In printing the electrode active material inks the layer thicknesses of 54 μm and 61 μm were achieved for the anode and cathode material, respectively. Both electrodes were designed for very high surface roughness (exceeding 20% of total layer thickness) in order to gain a high surface area on each electrode. Subsequently, the PET-film separator and the $ZnCl_2$ electrolyte were placed manually in-between the electrodes before sealing the separate half-cells together. The latter was achieved with a high performance adhesive tape, which had been previously attached to the paper substrate. Finally, the outer shape of the batteries was trimmed in order to expose the contact areas of the current collectors. A set of separate electrodes printed on plastic substrate and on paper FS-1 were also prepared for comparative resistance studies. Such electrodes were later analyzed also in closed

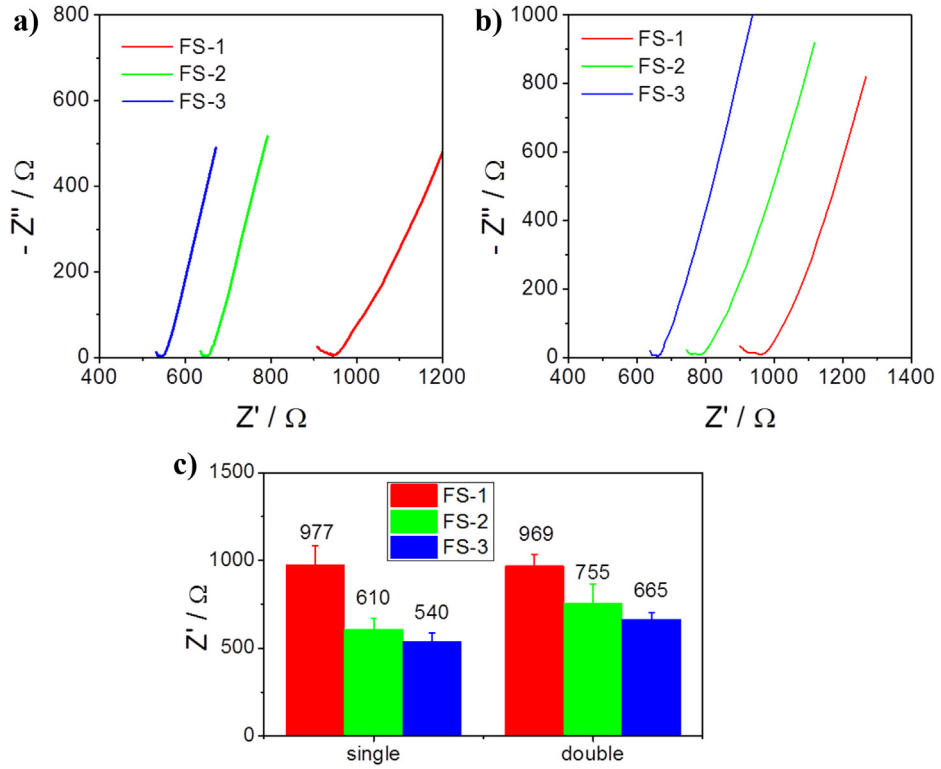

Fig. 2. Impedance spectra in the frequency range of 100 kHz–10 mHz at OCV of fresh (a) single cells and (b) double cells. (c) Values and scattering of the real part of impedance at high frequencies for the different configurations and battery series.

configuration after coating them with the gel electrolyte and assembling into a full cell using filter paper as separator.

Electrochemical investigations were based on galvanostatic discharge (GD) and electrochemical impedance spectroscopy (EIS) performed with a Bio-Logic VMP-3 potentiostat (Bio–Logic SAS, Claix, France) in two-electrodes configuration. Before EIS measurement the system was allowed to relax for 30 min and then the open circuit voltage (OCV) was applied to the cell for 15 min. When performing EIS measurements of fresh cells no waiting time was necessary and the OCV was directly applied for 15 min. The perturbation potential had an amplitude of 10 mV with frequencies ranging from 100 kHz to 10 mHz (10 points per decade). The conductivity of the open cells was measured in the frequency range of 100 kHz–1 kHz (10 points per decade). During the galvanostatic discharge a current of 100 μA was used to test the standard cells while a current of 1 mA was used for the optimized cell.

3. Results and discussion

The experimental evaluation of the thin-layer printed batteries can be divided into three parts: (1) study of the closed and sealed battery cells printed on paper coated with three different polymeric layers, (2) post-mortem analysis of those cells in order to verify the obtained results, and (3) analysis of open cells printed on paper FS-1 and plastic. The results of these investigations were used to optimize the printing procedure and the performance of the new improved cells was tested.

3.1. Investigation of the closed and sealed cells

Three series of batteries were analyzed (FS-1, FS-2 and FS-3), differing in the polymeric coating (barrier polymer), which function was to prevent the evaporation of the electrolyte and block the diffusion of oxygen. The samples of the examined series had rising transparencies according to the order FS-1 < FS-2 < FS-3. We attributed such difference in transparency mainly to the difference in base weight of the paper substrates.

EIS measurements on the fresh cells stressed that their overall cell impedance was higher than for batteries with standard current collector and dominated by the ohmic resistance of the system (see Fig. 2a–b). The ohmic resistance of the double cells was only slightly higher than for the single cells, while the value of the imaginary component of the impedance at low frequency of the 3.0 V batteries was twice higher than for 1.5 V cells, as expected from the series configuration. This evidenced that the highest

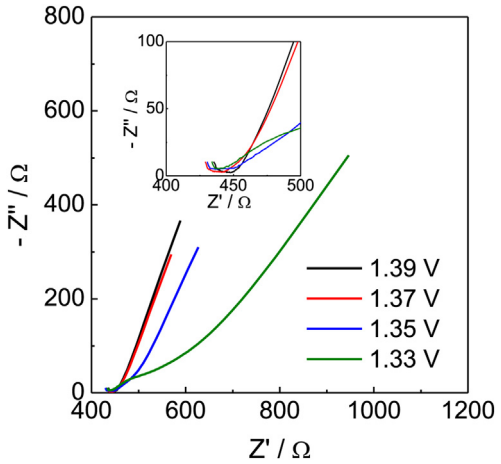

Fig. 3. Impedance spectra in the frequency range of 100 kHz–10 mHz of a 1.5 V battery (FS-3 series) recorded at different states of charge (potential reported after relaxation).

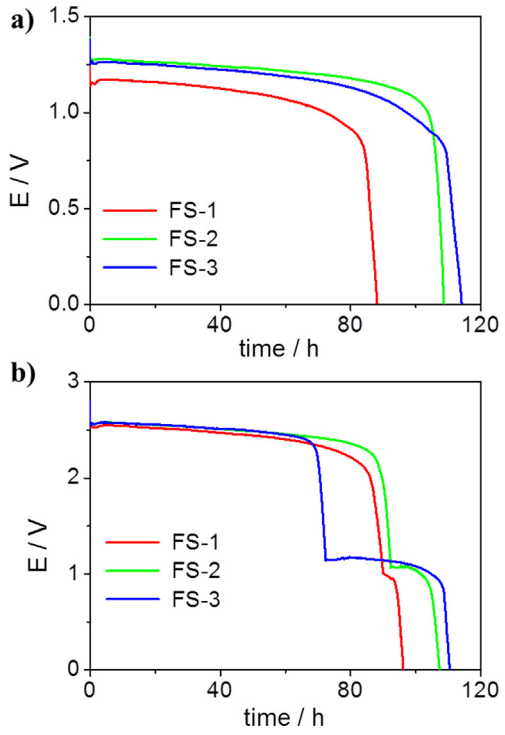

Fig. 4. Discharge profile at 100 μA of representative (a) single cells and (b) double cells for different battery series.

contribution to the overall cells impedance was arising from the external carbon connections (carbon contacts). The value of the real part of the impedance at high frequency was highly scattered, however, for the different series it remained in the order: FS-3 < FS-2 < FS-1 (see Fig. 2c).

To examine the changes in the battery impedance during discharge EIS experiments were performed at different states of charge. As expected, the impedance was changing with the state of charge. Initially, it was decreasing reaching a minimum at around the half of the discharge time. Thereafter, it was increasing again reaching the highest values after total discharge (see Fig. 3). Fig. 4a shows representative discharge profiles of the single cell of the different series. The shape of the discharge profile corresponds to a one-phase system with a constant sloping of the discharge curve [28]. The measurements of the open circuit voltage (OCV) showed that it was decreasing with the decreasing state of charge confirming a one-phase discharge mechanism [28]. Differences in the discharge time between series were observed when the same discharge current was imposed together with a strong scattering of the results among cells of the same series. Higher *iR* drop was observed for the cells with higher impedance. The best performing cells in each series, discharged at 100 μA, delivered a charge of 8.4, 10.5 and 10.9 mAh for the FS-1, FS-2 and FS-3 series, respectively. Assuming an apparent surface of the electrode of 3.8 cm^2, the specific charge density would be 2.2, 2.8 and 2.9 mAh cm^{-2}, respectively. Since the amount of electroactive material was kept the same in the three different series, the differences in extractable charge were likely related to the limited contact with the gel-electrolyte. This was also confirmed by post-mortem observations (see Paragraph 3.2).

The discharge profiles of the 3.0 V batteries were expected to be similar to their 1.5 V equivalents; however, as shown in Fig. 4b, the discharge profiles of the double cells at 100 μA current showed two plateaus, one at the expected potential of 2.5 V, the other around 1.0 V. This two-step discharge was caused by the difference in the extractable charge between the two cells connected in series. Thus, after the cell with lower charge was consumed, the voltage of the other cell drove a side reaction on the former, most likely electrolyte decomposition or further reduction of MnOOH to Mn_3O_4 [26]. Taking this mechanism into account, the overall charge of the single and double cells was comparable, as seen in Fig. 4a,b. Understanding the reason behind the premature discharge of the cells is essential to improve the utilization of the active material.

3.2. Post-mortem analysis of the discharged cells

Fig. 5 shows an example of the elements of the cells from different series after discharge. The active material in the FS-1 cells exhibited cracked areas, resulting from the more dry conditions within those cells caused by evaporation of the solvent. Some unused areas were remaining black after rinsing and drying of the cathodes (see Fig. 5) while the product of MnO_2 reduction (MnOOH) appeared white, as expected. This observation explains also the strong scattering in the charge of the different cells of the same series. In general, the electrolyte was spread on the surface of the Zn anodes uniformly. Because the inside of cells of the FS-1 series was much drier as compared to cells of the other series, the inhomogeneity in the electrolyte spread was more detrimental, while it was obviously a minor problem in the case of the FS-3 series. This is in agreement with the differences observed in the performance of the examined cells. In summary, inhomogeneous spread of the electrolyte, especially on the cathode side, was the main reason for the differences in charge between samples.

Measurements of the resistance between different points of the discharged electrodes and the carbon contacts were performed where possible. The most important observation was that the carbon contacts provide significant contribution to the

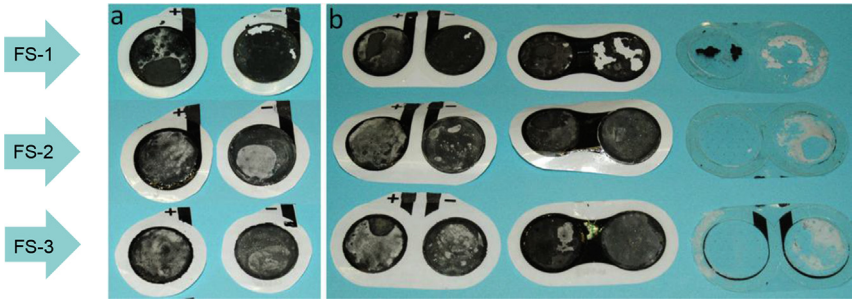

Fig. 5. Photographs of representative discharged electrodes for (a) single cell and (b) double cell configuration of different series. Manganese dioxide electrodes are signed with "+" and zinc electrodes with "−".

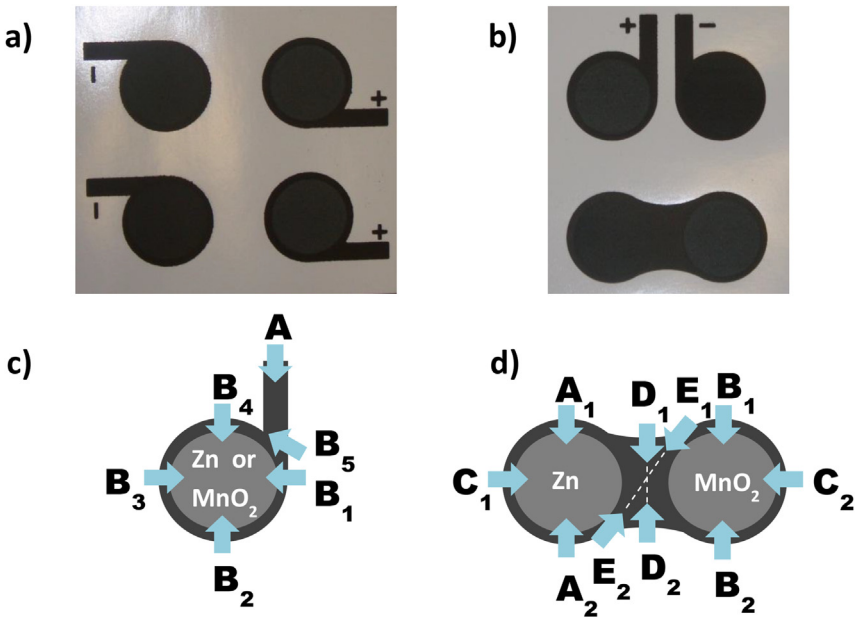

Fig. 6. (a) Single and (b) double open cells printed on paper (FS-1 series); (c) measuring points in the single cell; (d) measuring points in the double cell configuration.

overall electrode resistance, accounting for up to 60–70% of its total value at high frequency. It was also observed that the resistance of the carbon connections between the two cells connected in series in the double cells configuration was much lower than the resistance of the carbon contacts. This could explain why the ohmic resistance of the 3.0 V batteries was only slightly higher than that for the 1.5 V cells. These findings suggested that the improvement of the conductivity of the carbon contacts should be one focus towards the improvement of the overall battery performance.

3.3. *Investigation of the open cells*

Two sets of open printed batteries on paper (FS-1) and on a rigid plastic film were investigated without electrolyte (see Fig. 6a,b). The objective of the analysis of the open cells was to characterize the electric conductivity of the carbon current collector and contact and later to close them as in the previous experiments (Section 3.1) and examine the impedance spectra of the respective batteries. Conductivity experiments were performed in order to examine the resistance of the particular elements of the electrodes before they came in contact with the electrolyte. The sets of the results obtained from the resistance measurements for the cells printed on paper (FS-1) are shown in Table 1. Experiments were performed according to Fig. 6c–d in which the arrows indicate different sites of contact to the potentiostat. In accordance with the post-mortem analysis, the resistance of the carbon contacts of the fresh electrodes was very high (as shown in bold). Again, in the case of the double electrodes configuration (Fig. 6d), the resistance coming from the carbon connection (E_1–E_2) was about twice smaller as compared to the resistance of the carbon contacts of the single electrodes. This is due to the much wider paths of carbon connectors in the double electrodes configuration.

Conductivity experiments were also performed for the electrodes printed on plastic foil (Table 2). There was a clear difference between the results obtained for the two examined substrates due to the fact that the electric resistance of the carbon current collector printed on the plastic foil was about 5 times smaller than for the one printed on the paper substrate. The decrease in resistance for the plastic cells is in agreement with the increased thickness of the carbon layer.

To prove the importance of the electric resistance of the carbon current collector on the total impedance of the system, open cells printed on both substrates were wetted with the gel electrolyte, closed, and their impedance spectra were recorded (see Fig. 7). With increasing frequency, the impedance spectra show a semicircle which was attributed partially to the movement of the electrons inside the carbon current collector and the local reaction rates. It has also to be stressed that the value of the impedance measured at low frequencies for the fresh FS-1 cells (Fig. 7) was smaller as compared with the one measured for the aged cells (compare Fig. 2a).

Table 1
Resistance measured between different points of electrodes printed on FS-1 paper (see Fig. 7c,d). Values in bold show the resistance of the carbon contacts.

Resistance between marked sites/Ω				
2 electrodes set	Zn–MnO_2	single electrode	Zn	MnO_2
A_1–A_2	70	A–B_1	240	290
B_1–B_2	140	A–B_2	280	355
C_1–C_2	235	A–B_3	265	315
D_1–D_2	**85**	A–B_4	250	270
E_1–E_2	**100**	**A–B_5**	**200**	**225**
		B_1–B_3	75	140
		B_2–B_4	70	150

Table 2
Resistance measured between different points of electrodes printed on plastic (see Fig. 7c,d). Values in bold show the resistance of the carbon contacts.

Resistance between marked sites/Ω				
2 electrodes set	Zn–MnO_2	single electrode	Zn	MnO_2
A_1–A_2	28	A–B_1	57	76
B_1–B_2	80	A–B_2	69	90
C_1–C_2	88	A–B_3	69	87
D_1–D_2	**16**	A–B_4	59	74
E_1–E_2	**20**	**A–B_5**	**41**	**48**
		B_1–B_3	24	49
		B_2–B_4	26	70

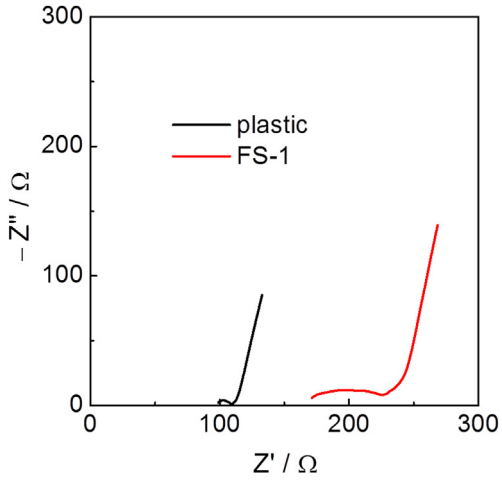

Fig. 7. Impedance spectra in the frequency range of 100 kHz–10 mHz at OCV of freshly assembled single cells on plastic substrate and paper FS-1.

3.4. Optimized printed battery

Based on the results described above, a new optimized cell was printed integrating a thicker carbon current collector and wider carbon contacts. The impedance spectrum of the fresh, optimized cell is shown in Fig. 8a, and it is striking that the value of the real component of the impedance is around one order of magnitude lower as compared with the value of similar cells before optimization (Fig. 2a). On the contrary, the imaginary part of the impedance is not strongly changed (around 1.5 times lower), indicating that the electro-active material is slightly better wetted in the optimized cell than in the old one. Being the impedance of such cell lower, it was tested with 1 mA. For comparison, also the old FS-3 cell was tested at 1 mA. The resulting discharge profiles are reported in Fig. 8b. Thanks to the optimization process, the power delivered by the battery at 1 mA raised from 0.32 mW to 1.25 mW.

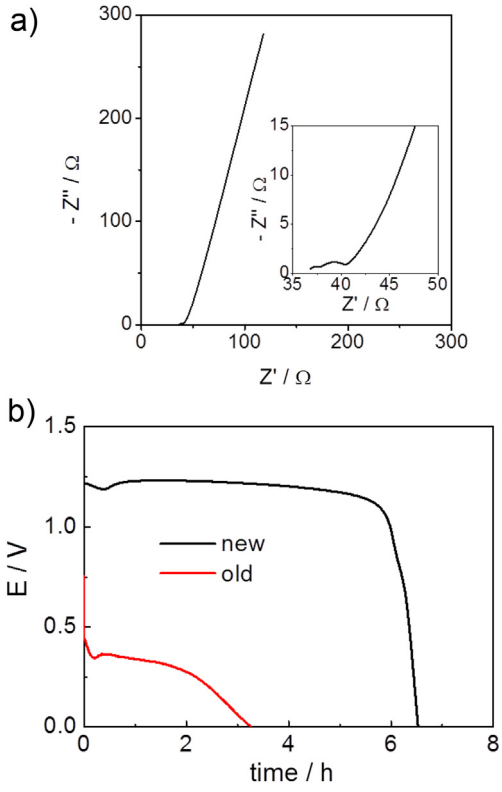

Fig. 8. (a) Impedance spectra in the frequency range of 100 kHz–10 mHz of the optimized battery at OCV. (b) Discharge profile at 1 mA of the representative optimized (new) and previous (old) single cell.

4. Conclusions

Several series of batteries printed on paper and plastic film substrates were investigated in order to pinpoint the main processes limiting the performances of the battery, and optimize them. It has been demonstrated that the high impedance observed for the paper batteries was due to the poor conductivity of the carbon current collectors, and the inhomogeneous spread of the gel electrolyte. Improvement of these parameters would decrease the overall impedance of the battery and enhance the performance of the cell upon discharge by raising the value of the operating voltage of the battery and increasing the discharge time, thus increasing the amount of extractable energy. It has been observed that in plastic cells, where the thickness of the carbon current collector was higher, the electric resistance was smaller. Based on these observations, an optimized cell was fabricated and analyzed. The main improvement was thickening and widening of the carbon current collectors in order to decrease the internal resistance of the cells. The optimized cell showed a decrease in the value of the real part of the impedance at high frequencies of one order of magnitude and a 4-fold improvement in the power delivered during discharge at 1 mA.

Acknowledgments

Financial support by the Federal Ministry of Education and Research (BMBF) in the framework of the project “BatMat” (FKZ 13N11399) as well as the funding of the Centre for Electrochemical Sciences (CES) by the European Commission and the state North Rhine-Westphalia (NRW) in the framework of the HighTech.NRW program are gratefully acknowledged. The authors are thankful to Schoeller Technocell GmbH & Co. KG for providing the paper substrates.

References

[1] V.L. Pushparaj, M.M. Shaijumon, A. Kumar, S. Murugesan, L. Ci, R. Vajtai, R.J. Linhardt, O. Nalamasu, P.M. Ajayan, Proc. Natl. Acad. Sci. U. S. A. 104 (2007) 13574–13577.
[2] L. Hu, J.W. Choi, Y. Yang, S. Jeong, F. La Mantia, L.-F. Cui, Y. Cui, Proc. Natl. Acad. Sci. U. S. A. 106 (2009) 21490–21494.
[3] M. Kaempgen, C.K. Chan, J. Ma, Y. Cui, G. Gruner, Nano Lett. 9 (2009) 1872–1876.
[4] D.-H. Kim, Y.-S. Kim, J. Wu, Z. Liu, J. Song, H.-S. Kim, Y.Y. Huang, K.-C. Hwang, J.A. Rogers, Adv. Mater. 21 (2009) 3703–3707.
[5] M. Wendler, G. Hübner, M. Krebs, Int. Circular Graph. Educ. Res. 4 (2011) 32–41.
[6] C.C. Ho, J.W. Evans, P.K. Wright, J. Micromech. Microeng. 20 (2010) 104009.
[7] M. Hilder, B. Winther-Jensen, N. Clark, J. Power Sources 194 (2009) 1135–1141.
[8] K.T. Braam, S.K. Volkman, V. Subramanian, J. Power Sources 199 (2012) 367–372.
[9] W.G. Tam, J.S. Wainright, J. Power Sources 165 (2007) 481–488.
[10] L. Hu, H. Wu, F. La Mantia, Y. Yang, Y. Cui, ACS Nano 4 (2010) 5843–5848.
[11] T. Janoschka, A. Teichler, B. Häupler, T. Jähnert, M.D. Hager, U.S. Schubert, Adv. Energy Mater. 3 (2013) 1025–1028.
[12] R. Bhattacharya, M.M. de Kok, J. Zhou, Appl. Phys. Lett. 95 (2009) 223305.
[13] P. Chen, H. Chen, J. Qiu, C. Zhou, Nano Res. 3 (2010) 594–603.
[14] A. Laforgue, J. Power Sources 196 (2011) 559–564.
[15] M. Pasta, F. La Mantia, L. Hu, H.D. Deshazer, Y. Cui, Nano Res. 3 (2010) 452–458.
[16] L. Hu, F. La Mantia, H. Wu, X. Xie, J. McDonough, M. Pasta, Y. Cui, Adv. Energy Mater. 1 (2011) 1012–1017.

[17] D. Linden, T.B. Reddy (Eds.), Handbook of Batteries, third ed., McGraw-Hill, New York, 2001.
[18] E. Barsoukov, J. Kim, D. Kim, K. Hwang, C. Yoon, H. Lee, J. New Mater. Electrochem. Syst. 4 (2000) 303–310.
[19] T. Patey, A. Hintennach, F. La Mantia, P. Novák, J. Power Sources 189 (2009) 590–593.
[20] J. Jespersen, A. Tønnesen, K. Nørregaard, L. Overgaard, F. Elefsen, World Electr. Veh. J. 3 (2009).
[21] H. Kipphan, Handbuch der Printmedien – Technologien und Produktionsverfahren, Springer Verlag, Berlin, 2000, p. 401.
[22] A. Willert, A. Kreutzer, U. Geyer, R. Baumann (Eds.), Smart Systems Integration 2009 – 3rd European Conference & Exhibition on Integration Issues of Miniaturized Systems, March 10–11, 2009, Brussels, AKA Verlag, Heidelberg, 2009, pp. 556–559.
[23] A. Rombold, Siebdruck und Serigraphie, E.A. Seemann Verlag, Leipzig, 1995, pp. 7–47.
[24] J. Böhringer, P. Bühler, P. Schlaich, Kompendium der Mediengestaltung. Produktion und Technik für Digital- und Printmedien, Springer-Verlag, Berlin, Heidelberg, 2011, pp. 601–603, http://dx.doi.org/10.1007/978-3-642-20582-8_9.
[25] H. Scheer, Siebdruck-Handbuch, Verlag Der Siebdruck, Lübeck, 2007, p. 33.
[26] D.W. McComsey, in: D. Linden, T.B. Reddy (Eds.), Handbook of Batteries, third ed., McGraw-Hill, New York, 2001, pp. 171–215.
[27] W. Schmidt, in: 23rd International Conference on Digital Printing Technologies: Digital Fabrication, September 16–21, 2007, Anchorage, IS&T, Springfield, 2007, pp. 923–924.
[28] A. Kozawa, R.A. Powers, J. Chem. Educ. 49 (1972) 587–591.